Localized Intensification of Arsenic Release within the Emergent Rice Rhizosphere

Yin, Daixia; Fang, Wen ; Guan, Dongxing; Williams, Paul; Moreno-Jimenez, Eduardo; Gao, Yue; Zhao, Fangjie; Ma, Lina; Zhang, Hao; Luo, Jun

Published in:
Environmental Science and Technology

DOI:
10.1021/acs.est.9b04819

Publication date:
2020

Localized intensification of arsenic release within the emergent rice rhizosphere

Dai-Xia Yin,[†] Wen Fang,[†] Dong-Xing Guan,[†] Paul N. Williams,[‡,*] Eduardo Moreno-Jimenez,[§] Yue Gao, [∥] Fang-Jie Zhao,[⊥] Lena Q. Ma, [†,#] Hao Zhang, [¶] Jun Luo [†,*]

[†]State Key Laboratory of Pollution Control and Resource Reuse, School of the Environment, Nanjing University, Nanjing, Jiangsu 210023, China

[‡]Institute for Global Food Security, School of Biological Sciences, Queen's University Belfast, Belfast BT9 5DL, Northern Ireland, United Kingdom

[§]Department of Agricultural and Food Chemistry, Universidad Autónoma de Madrid, E-28049 Madrid, Spain

[∥] Analytical, Environmental and Geochemistry (AMGC), Faculty of Science, Vrije Universiteit Brussel, Pleinlaan 2, Brussels, Belgium

[⊥] Jiangsu Collaborative Innovation Center for Solid Organic Waste Resource Utilization, College of Resources and Environmental Sciences, Nanjing Agricultural University, Nanjing, Jiangsu 210095, China

[#]Soil and Water Science Department, University of Florida, Gainesville, FL 32611, USA

[¶] Lancaster Environment Centre, Lancaster University, Lancaster, LA1 4YQ, UK

* Corresponding authors: Jun Luo, 0086-25-89680632, esluojun@nju.edu.cn; Paul N. Williams, p.williams@qub.ac.uk

21 TOC

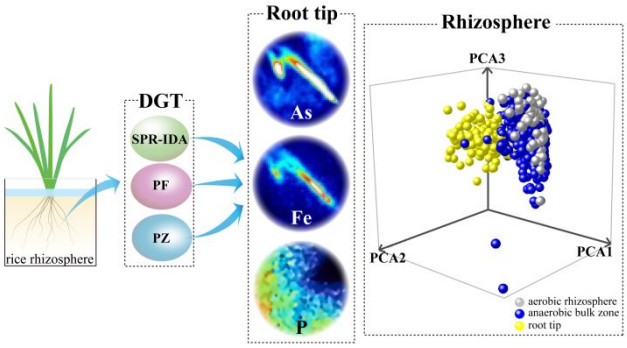
rice rhizosphere
DGT
SPR-IDA
PF
PZ
Root tip
As
Fe
P
Rhizosphere
PCA3
PCA2
PCA1
aerobic rhizosphere
anaerobic bulk zone
root tip

22

ABSTRACT

Trace element behavior in flooded/lowland rice soils, is controlled by root-zone iron oxidation. Insoluble iron species bind/capture toxic elements, i.e. arsenic. However, it was recently observed that within this territory of arsenic immobilization lies a zone of prolific iron release, accompanied by a significant flux of arsenic in close proximity to rice root apices. Questions still remain on how common this phenomenon is and whether the chemical imaging approach or soils/cultivars used influence this event. Here, three types of ultra-thin/high-resolution diffusive-gradients-in-thin-films (DGT) substrates, were integrated with oxygen-planar-optodes into a sandwich-sensor, providing a two-dimensional mapping of solute fluxes. The three DGT approaches revealed a consistent/overlapping spatial distribution with localized flux-maxima for arsenic, which occurred in all experiments, concomitant with iron mobilization. Soil/porewater micro-sampling within the rhizosphere, revealed no significant elevation in the solid phase's total iron and arsenic concentration between aerobic and anaerobic zones. Contrary to arsenic, phosphorus bioavailability was shown to decrease in the arsenic/iron flux-maxima. Rice roots, in addition to their role in nutrient acquisition, also perform a key sensory function. Flux-maxima represent a significant departure from the chemical conditions of the bulk/field environment, but our observations of a complete rhizosphere reveal a mixed-mode of root-soil interactions.

INTRODUCTION

Arsenic (As) is a well-established poison with human carcinogenic properties. Dietary exposure to this toxic element remains a major global health issue.[1-3] Continual inputs of As enter our agri-food systems either via atmospheric deposition and/or via geological supply.[4] However, this transfer has intensified with anthropogenic processes such as mining, waste incineration, fertilizer use, fossil fuel combustion, and irrigation with As-enriched water[3]. Importantly, As bioavailability in soil is enhanced with increasing temperature. Future climate-change scenarios predict a doubling in rice grain As by 2100[5] compared to the present day.[1] Plant uptake of As is accidental, occurring via transport systems that evolved for the absorbance of phosphorus (P)[6,7] and silicon (Si).[8] As a wetland crop, rice efficiently accumulates As that is readily liberated under the highly reducing conditions of rice paddy.[9] This poses, then, a serious health risk to consumers for which rice is the staple food.[10]

Improvements to our understanding of where and how As mobilizes and interacts with other elements, especially iron (Fe) and manganese (Mn), within the rice rhizosphere is needed for more targeted root-soil management.[9,11] For example, release of oxygen (O_2) from the aerenchyma of rice roots into the rhizosphere can cause Fe(II) oxidation and Fe (hydr)oxide deposition around roots and thus decrease soluble As.[12] Furthermore, Mn oxides can enhance As adsorption onto indigenous Fe (hydr)oxide phases, by promoting the oxidation of As(III) to As(V) and thus greatly reducing the porewater As concentration in the rice rhizosphere.[13,14] The rooting zone in lowland

66 flooded rice, though, is a particularly complex and only partially understood
67 environment. Processes such as the release of exudates and mineral nutrient weathering,
68 adsorption/desorption of ions from colloids, and the formation of precipitates and
69 organic-inorganic complexes all contribute to make a patchwork of highly diverse and
70 spatially-changeable chemistries.[15] However, it is the differences in redox conditions,
71 and the radial O_2 loss (ROL) from rice roots especially that alter elemental speciation
72 and bioavailability.[16,17] For example, ROL leads to great variation in pH, Eh,
73 Fe(III)/Fe(II) quotients within micrometer ranges from root surfaces, which impact on
74 Fe plaque formation and metal fractionation and mobility.[18,19] Also, the proportion of
75 active microbial communities in the rhizosphere are 2-20 times higher than in the
76 corresponding bulk/field soil,[20] further intensifying the chemical reactivity within the
77 rooting zone.[21,22]

78 Encompassing a relatively small volume of soil, most rhizospheres only extend out
79 on a millimetre scale from their associated roots.[23] The reach of the rooting zone, in
80 aquatic plants such as rice though can range further because of ROL. [24,25] However, due
81 to these zones being so redox sensitive, the chemistry in these regions is highly
82 susceptible to disturbances arising from sampling. It is therefore necessary to develop
83 methods that are of an appropriately high-resolution (HR), in the sub-millimeter scaling
84 range, that can function with minimal impact on the biophysico-chemical processes
85 occurring *in situ*. Traditional rhizobox and root-mat approaches for studying
86 rhizosphere heterogeneity are challenged by the narrow spatial gradients produced by
87 rhizosphere processes around roots,[26] and for not being purpose designed/built for

flooded soil conditions. An alternative approach is to use DGT-optode "multilayer systems". Diffusive gradients in thin films (DGT), a passive sampling technique, can measure labile metals and metalloids to predict plant availability in water, sediment and flooded soils.[27,28] Two-dimensional (2D) luminescent imaging techniques (planar optodes) have been applied to measure O_2/pH/CO_2 dynamics in a range of environments, which includes rhizospheres and soils.[9, 25] These technologies were coupled to study the behavior of TE's in wetland soils and sediments,[29] and also applied to aquatic plant rhizospheres, such as seagrass and rice.[9,30,31] Consisting of a pH/O_2-sensitive planar optode, backed by an ultrathin (60 μm) DGT layer for capturing labile TE fluxes, the HR DGT binding gel can measure/visualize metal solute chemistries with resolutions up to ~100 μm.[32] Not only are the individual metal/element/pH/O_2 distribution images useful for interpreting the spatial lability trends, but viewed together can provide insight into the modes/mechanisms of solute release as well.[9] During, these initial experiments an unexpected pulse of labile As, along with Fe and lead (Pb), was observed congruent to that of the peripherals of the aerobic rhizosphere zone.[9] However, the soils used in that study, contained a low concentration of As (2 mg kg^{-1}). Furthermore, although the rhizotrons were conditioned as wetlands, the soil used was not sourced from a rice paddy. So, whether the As mobilization trend could be replicated in an actual rice soil remains unresolved.

In the chemically dynamic environment of the rice rhizosphere, multiple element-element interactions and diffusion-oxidation reactions would be overlaid. The DGT as a receptor to these fluxes, provides a time integrated summation of these processes.

110 However, it is posited that by altering the chemistry of this sink, a different image or
111 time lapse photograph in a single frame,[33] would be captured. Therefore, in this study,
112 sandwich-sensor solute mapping of the rice porewater was performed using three DGT
113 binding substrates; precipitated ferrihydrite, precipitated zirconia and suspended
114 particulate reagent−iminodiacetate (SPR−IDA), alongside standard micro-sampling of
115 soils/waters. As a continuation of previous work,[9] this experiment was designed to
116 further test the distribution/commonalities in element bioavailability in rice
117 rhizospheres developed in actual paddy soil, with elevated As concentrations. In
118 addition, the scale of the solute mapping was expanded from ~400 mm^2,[9] to over 3000
119 mm^2 to capture localized solute behaviors across multiple roots simultaneously. Finally,
120 because of the close association between Fe and P mobilization, and the ability of the
121 new DGT samplers to simultaneously measure Fe, As and P, it was possible to test
122 whether the chemical hotspots around the root tips also represented sites of significant
123 P supply.

124 Our hypotheses included: i) flux maxima in As, Fe mobilization at the apice zones
125 of the rhizosphere in flooded lowland rice are common in different growing
126 environments, ii) metal, As, P fluxes can be detected by DGT samplers configured with
127 different binding layers, i.e. the mobilization patterns are not an artifact of a single gel
128 type, iii) that the porewater trends are a result of either porewater diffusion and soil-
129 water interactions, rather than general element enrichment of the soils in the aerobic
130 rhizosphere.

131

EXPERIMENTAL SECTION

Method Summary. Three different ultrathin/HR DGT configurations, with a thickness of 60 μm were mounted on 2D O_2 optodes and exposed to preflooded and conditioned rice rhizotrons, following a previously described method.[9] Furthermore, sampling of soil and porewaters was undertaken across a series of identical rice rhizotrons to observe the general trends associated with rhizosphere development, guided by O_2 profiles obtained via optode measurement.

Soil and Rice Cultivation. The paddy soil was collected in the region of Extremadura (SW of Spain, 39°06'N; 5°40'W), the second biggest producer of rice in Spain. The soil, an Hydragric Anthrosol, has a loam texture, having formed in a Mediterranean climate, with hot and dry summers, 500 mm of annual rainfall and an aridity index of 0.5. It has an acidic to circumneutral soil pH, unlike other paddy regions in Spain that are predominantly basic. The soil contained ~17 mg As kg^{-1} (determined by ED-XRF, see SI Table S1), which is above the global average for As in soil,[34] and considerably more elevated than the soils used in Williams et al. (2014)[9]. A compilation of relevant element concentrations can be found in the Supporting Information (SI) (Table S1). The soils were air dried and passed through a 2 mm sieve before packing into rhizotrons. For the rhizotron experiment, rice plants were pre-cultured in nutrient solution for two weeks before being transplanted to the rhizotrons. More specifically, after sterilization in 0.5% NaOCl for 10 min, rice seeds were soaked in deionized water overnight and germinated at 25 °C for 2 days. Seedlings were transferred to a nylon net floating on 1/2 strength Hoagland's solution in a greenhouse. After 2 weeks, rice

154 seedlings were transferred to the prepared rhizotrons for a further 2 weeks growth.

155 **DGT Preparation.** In the rhizotron experiments, three different ultra-thin DGT
156 substrates were used for chemical imaging: suspended particulate reagent-
157 iminodiacetate (SPR-IDA),[35] precipitated ferrihydrite (PF),[36] and precipitated zirconia
158 (PZ).[37] DGT measures fluxes and interfacial concentration based on kinetic rather than
159 equilibrium principles. The performance of ultra-thin DGT has been verified and SPR-
160 IDA gel possesses adequate adsorption capacity (e.g. Cd is 0.26 mg) for cations and
161 some anions.[35,38] Meanwhile, PF and PZ gel exhibit stronger adsorption capacity for
162 anions in preference to cations.[36,37] The fast uptake of the target ions to the PF (binding
163 rate for As is 0.011 μg cm^{-2} min^{-1}) and PZ gels (binding rate is 0.003 μg cm^{-2} min^{-1})
164 has previously been verified.[36,37] However, there are limitations for SPR-IDA resin gels,
165 especially for anion measurement. Their performance depends on solution conditions[35]
166 and not all species, such as As(V), are captured quantitatively.[32] Adsorption−desorption
167 of As is the primary factor that impacts on the bioavailability and mobility of As in
168 soils. Metal ligands bind with a distribution of *K* values, resulting in a range of labilities
169 for bound metals that is affected by the extent of binding. Although, differences in
170 ligand-assisted dissociation of complexes in different resin layers has an important role
171 on the binding performance,[39] different binding layers also represent different sinks that
172 could potentially alter the final chemical image based on binding characteristics. This
173 idea was further explored in this study.

174 The SPR-IDA gels were prepared as described before.[9] Briefly, 1 ml SPR-IDA
175 suspension was added to 1 ml mixture of acrylamide (40%, BDH Eletran) and agarose-

derived cross-linker (DGT Research Ltd., UK) (40% acrylamide/cross-linker, 4/1). Then 14 μL of ammonium persulfate (BDH) and 4 μL of *N,N,N',N'*-tetramethylethylenediamine (TEMED) (BDH Electran®) were added. After quick mixing, the gel solution was then immediately cast between two glass plates separated by a 0.06 mm plastic spacer. Once cast, the glass plate was assembled and placed into an oven at 45 ^{o}C for 1 h. Afterwards, the glass plates were separated, and the gels was placed into 0.5 L of ultrapure water (MQ water, Millipore, 18.2 MΩ) and allowed to fully hydrate for at least 24 h with water changing 3-4 times.

To prepare the PF and PZ gels, a series of ultra-thin acrylamide gels, following the same protocols as the SPR-IDA but without the binder, were cast using 0.06 mm thick spacers. After hydration, the gel sheets were immersed in solutions of 100 mL 0.1 M $Fe(NO_3)_3 \cdot 9H_2O$ or 0.1 M $ZrOCl_2 \cdot 8H_2O$ for PF gels[36] and PZ gels[37], respectively. These gels were immersed for at least 2 h to ensure a uniform distribution of Fe or Zr in the matrix. Afterwards, each gel was rinsed with MQ water for 1-2 s and then immersed in 100 mL of 0.05 M 2-(*N*-morpholino) ethanesulfonic acid (MES, biochemical, BDH) buffer solution (pH 6.7) to produce a precipitation of ferrihydrite or zirconia directly into the gels. After about 40 min of shaking gels to allow complete development, the gels were rinsed several times in MQ water, and soaked in MQ water for 24 h. Over this period the water bath was changed 5-6 times.

All preparation and processing of gels was conducted in a laminar flow bench (SW-CJ-1B, Airtech, China) within a clean room using ultraclean trace metal techniques. Before deployment, acid-washed Nuclepore membranes (Nucleopore,

198 Whatman, 0.4 μm pore size and 10 μm thickness) were fixed between the soil and gel,
199 to avoid particle contamination, and to act as a diffusion layer for the DGT binding gel.
200 All binding gels were preserved in 0.01 M NaCl solution until rhizosphere deployment.

201 **Rhizotron Experiment**. The plant-soil housings used in this study had inner
202 dimensions of 40cm×10cm×1.5cm (height×length×width), with detachable front plates,
203 that were filled with the sieved soils. The soils were compacted in layers to achieve a
204 homogeneous texture with a uniform bulk density of 1.3 kg L^{-1}. Soils in rhizotrons were
205 carefully saturated with water using a slow-flow gravimetric irrigation system, to avoid
206 disturbing the soil structure and to enable Nuclepore membranes (pore size is 0.2 μm
207 and thickness is ~10 μm) to be fixed on the ventral plane of the rhizotron. The
208 membranes help to ensure soil uniformity during DGT and planar optode deployment
209 and protect the roots and soils from being disturbed when the rhizotron's front plates
210 were later removed. The filled rhizotrons were then conditioned anaerobically in a
211 water tank purged with nitrogen gas, for 2 weeks, after which, a 2-week-old rice
212 seedling (cv. Nipponbare), was transplanted in close proximity to the front plate of each
213 rhizotron. The planted rhizotron systems were maintained at a 30-45^{o} inclination to
214 facilitate the root growth along the lower front windows of the devices. In total, 14
215 rhizotrons were prepared. The rooting/soil zones in all the replicates were kept away
216 from light to simulate field conditions and avoid inducing microphyte growth. Plant
217 development was monitored frequently, with root development assessed by visual
218 inspections and O_2 measurements from planar optodes (detailed descriptions are
219 presented in the SI). At the time of sampling (4-week-old seedlings) the replicates with

220 the clearest ROL profiles were selected for 2D solute/chemical imaging by the
221 combined DGT/optode sampler. After the DGT/optode retrieval, the destructive
222 sampling for porewater and subsoils in all rhizotrons was conducted as below.

223 **Chemical Mapping**. After 24 h deployment in the rhizotrons, the DGT gels were
224 retrieved and rinsed with MQ water, and dried using a gel drier (Bio-Rad model 543)
225 and then carefully fixed onto glass plates using heat-resistant double-sided adhesive
226 tape prior to laser ablation (New Wave, Cambridge, U.K.) coupled with inductively
227 coupled plasma mass spectrometry (NexION 300, PerkinElmer, USA) (LA-ICP-MS)
228 analysis. Calibration and detector performance were optimized prior to commencing
229 dry plasma tuning. The laser system, with wavelength quadrupoled to 213 mm, was
230 equipped with a large format ablation cell. Line scans of the gels were carried out at a
231 spot size of 100 μm, scanning speed of 100 μm s^{-1}, an interline spacing of 400 μm, a
232 repetition rate of 20 Hz, and energy output is 0.012 J cm^{-2}. ICP-MS was used to record
233 the elemental signals (Table S2). ^{13}C was used as internal standards to correct variations
234 in ablation, transport, and ionization efficiency.

235 O_2 distributions in the rhizotrons were captured using planar optode sensors.[40]
236 Procedures of optode fabrication and imaging are presented in the SI. Processing of the
237 original DGT data was conducted firstly in Microsoft Excel 2016 and then ImageJ 1.50i,
238 whereas optode data was processed directly in ImageJ 1.50i. Principle Components
239 Analysis (PCA) of transects of the main images were conducted in Minitab19.

240

Rhizotron Soil and Porewater Sampling. To collect soils and porewaters during plant harvesting, we used a compartmented approach targeting bulk/field anaerobic and rhizosphere aerobic soil zones, as determined by planar optode measurements. Sampling was conducted in an aerobic cabinet (YQX-II; Longyue), purged with nitrogen (>99.5%) to stabilize the redox conditions. Concentrations of O_2 within the main chamber, which contains vessels of desiccant and deoxidizer catalyst, were 0.01% after a standard N-purge of 1 h. Porewater were extracted by applying suction to Rhizon samplers (0.15μm pore size, 1mm outer diameter, and 8mm long, No. 19.21.81, Rhizosphere Research Products, Netherlands) using syringes, after the samplers were inserted into soils and left to equilibrate for 1 h. The collected porewaters were then acidified with high purity HNO_3 and analysed by ICP-MS.

The fresh soil samples (~3 g) were collected using a plastic spatula, then freeze-dried and sieved (2 mm). Subsamples of 0.2 g were digested in a mixture of HNO_3 and H_2O_2 (EPA 3050B) and then element concentrations were analysed using ICP-MS, for more details on the quality assurance and quality control see the SI (Table S3).

RESULTS AND DISCUSSION

Localized Intensification of As Mobilization across the Rhizosphere-Soil Continuum is a Common Occurrence. In support of previous observations,[9] the rhizospheres formed by the seedlings were found to have a demonstrable effect on the occurrence and intensity of both O_2 and element fluxes. This is clearly shown in Figures 1 and S2 (see SI), where oxygenation is sustained most effectively in the central

262 rhizosphere, dissipating as the peripheries of the root zone were reached. As the
263 interpretation here of the rooting zone is based on the optode images, a more appropriate
264 term would be the aerobic rhizosphere (**O+R**). Conversely, O_2 concentrations in the
265 surrounding bulk/field soil were barely detectable, indicating the general soil
266 environment (**O-B**) was anaerobic/highly reducing. The **O+R** can lie in very close
267 proximity to the root surface, but it is not exclusively so, and oxic conditions can form
268 up to several millimetres away from roots. These aerobic pockets can be maintained by
269 a variety of processes that include: continual radial O_2 diffusion from the roots, as well
270 as there being potentially also some O_2 drawn down from the aerobic overlying waters,
271 as the channels in the soils formed by the roots form a conduit to the surface.[41]

272 As previously observed,[9] the flux images with SPR-IDA DGT illustrate a general
273 commonality in the spatial distribution of As, Fe and Pb (Figure 1 and S2, Table 1), but
274 also a series of subtle differences. A key similarity was that flux maxima (**FM**) for all
275 three elements converged in regions associated with root apex rhizosphere zones. One,
276 **FM1** in Figure 1c) occupied ~1.5 x 0.5 cm^2 and comprised of two distinct branches.
277 The second zone (**FM2** in Figure 1c), was less prominent but exhibited similar chemical
278 features. Interestingly, there were no flux maxima or ROL associated with the primary
279 root in the **O-B** zone, with As bioavailability around this feature actually recording a
280 lower flux than the surrounding non-rhizosphere/anaerobic soil (Table 1). On the
281 contrary, the **O+R** appeared to have a limited impact on the bioavailability of Mn. There
282 was some Mn release where the Fe/As root maxima located. However, these fluxes
283 were only slightly above background and notably less intense than the microniche

features (Figure 1e). However, Mn was mobile, with release characterized as a widespread series of discrete hotspots, with a typical size of 0.4 mm^2. Within this dispersed array of Mn microsites, four larger, roughly spherical maxima clustered in the upper soil zone (**M1**, Figure 1e), indicating a slightly different mode of release. Variations in oxidation rate and biological activity under flood conditions would affect Mn behavior, with a variety of microorganisms known to be capable of coupling growth to Mn oxide reduction, using Mn as a terminal electron acceptor. In addition to Mn(II), soluble Mn(III) or Mn(IV)[42,43] would also be targeted by DGT, so the measurements are a multi-species summation. However, Mn(II), is a simple/hydrated species, and once formed is more stable in anoxic water than Fe(II).[44]

Spatial flux patterns of Co, Ni, and Zn did not map with either the **O+R** or **FM** rhizosphere. However, there was a clear association between the Co, Ni, Zn and Mn observed in a Principle Components Analysis (PCA) of a transect encompassing **FM1**, **O+R1**, and **O-B1** regions (Figure 1f). The PCA, also highlights a clear differentiation in chemistries/flux characteristics between the zones (Figure 1f).

When the experiment was repeated but with a new rhizotron/seedling, a similar but less obvious series of root tip maxima for As, Fe and Pb were also observed (**FM3** & **FM4** in Figure 2). Again, the enhanced mobilization was constrained to the upper root zones and showed a similar pattern to that of the main fluxes in Figure 1. Fluxes of As, Fe and Pb around the tips were different from either the **O+R** zone or anaerobic bulk/field soil (PCA, Figure S3). However, interestingly, for **O+R2** (Figure 2), the mobilization patterns for As and Fe were different to **O+R1** (Figure 1) and previous

306 results[9] turning this region into a flux hotspot compared with the surrounding anaerobic
307 bulk/field soil. Reasons for this could be due to the oxic zone, being less developed and
308 more unstable than in the rhizosphere captured in Figure 1. Furthermore, trends in As
309 and Fe mobilization were consistent, but Pb release was unconnected. Indeed, the
310 feature **O+R2** shares many chemical similarities to the root flux maxima zones but with
311 less intense element lability and a larger spatial coverage. Again, there were Mn hotspot
312 maxima as well as depletion features, but they bared little relationship to the **O+R** zones
313 (Figure 1 and 2).

314 In another region of chemical relevance (microniche-**M2**; Figure 2), observed
315 within the anaerobic bulk/field soil, the average fluxes of Fe and Mn were greater than
316 the surrounding soil reaching up to 6.31 and 0.42 pg cm^{-2} s^{-1} respectively (baseline
317 levels being 3.70 and 0.17 pg cm^{-2} s^{-1} respectively). This result is consistent with
318 previous findings,[9] which also observed a microniche with a similar flux pattern for Fe
319 and Mn. Microniches principally form because of microbial driven
320 mobilization/depletion of metals, often catalyzed by the hotspot having different rates
321 of organic carbon decomposition/mineralization and/or different microbial
322 communities, compared with the surrounding soils.[45] Products of microbial metabolism
323 and synthesis, especially, can contribute to metal mobility.[46] For example, Fe flux
324 maxima may be caused by Fe reducing bacteria mediated reductive dissolution. The
325 organic matter from root exudates can also serve as an electron donor for Fe reduction.
326 It promotes the dissimilatory reduction of adsorbed As(V) by dissimilatory arsenate-
327 reducing bacteria and releases As into the aqueous phase.[47]

Based on Pearson correlation analysis there are significantly positive correlations between As and Fe fluxes on SPR-IDA DGT across the root tip zones (p<0.01, Figure S4), indicating a close association between the two elements. Although Pb also exhibits a strong positive relationship with As and Fe, two different correlation patterns emerge. One associates with the center of the flux feature, the other a surrounding/bordering zone in close proximity to the periphery of the maxima and **O+R** zone. Interestingly, there is also a stronger association between the supply of Pb and Mn in this edge region. Manganese hydroxides are superior scavengers of Pb compared with other metal hydroxides, and are about ~40 times more effective as an adsorbent of Pb than FeOH,[48] but a general lack of co-localized release of Mn and Pb in this studied plant-soil system suggests this is not a dominant reaction state. Metal-oxide ternary complexes can also influence bioavailability, especially in carbon rich environments, and determine if metal adsorption at oxide surfaces is enhanced or inhibited by the presence of ligands.[48] In the dynamic environments of root apices and flux maxima the spatial variability we document reveals the potential for a wide range of metal/ligand ratios to exist even within a confined area.

The Flux Comparison between Different DGT Gels. Consistent with the SPR-IDA-gel ion maps, both the PZ and PF-based DGT's (Figure 3 & 4) also revealed a co-occurrence of As and Fe flux maxima, and that this was associated with upper/shallower root apice zones of the rhizosphere. For PZ gel (Figure 3), enhanced metal fluxes were evident along the aerobic-anaerobic interface, but the flux maxima in the tip zone remained the strongest/most intense region of As and Fe supply. Concentrations of

labile As inside the **O+R** were consistently low, ranging between 1-1.4 $pg \cdot cm^3 \cdot s^{-1}$. The same trends were detected by PF gels (Figure 4). Fluxes of As were strongest within the rhizosphere of the root tip, not where O_2 intensity was greatest but in a transition zone of relatively unstable aeration. This is consistent with the solute images captured by the SPR-IDA DGT and previous studies.[9,49]

In contrast to As and Fe, a relatively low flux of P occurred within the **O+R** (Figure 3&4), which might be ascribed, in part, to its rapid depletion by root uptake,[50] and/or fixation by Fe plaque.[51] The fluxes of P at RTA are 54% lower than the bulk/field soil area as measured by the PF DGT, and 79% less based on PZ DGT detection. Absorption of P, in most plants, is constrained by kinetics, but under conditions of unhindered diffusion from **O-B**/bulk/field soils to the root-soil interface uptake is rapid.[52] However, the patterns of low P mobilization/depletion do not follow the root system directly. Instead they map more closely to the edges of the **O+R**, suggesting the importance of redox rather than root exudates as an overarching/primary control on P availability. The role of redox conditions as a determinant of P availability is further evidenced by DGT being a poor indicator of P availability in rice, when the redox potentials of tested soils are not representative of field conditions.[53] Oxidation is a major contributor to acidification within the rooting zone and rhizosphere acidification plays a key role in P acquisition by rice.[50] Furthermore, P also modulates the behaviors of the other elements, such as Pb, with Pb-phosphate being one of the most insoluble forms of Pb in soil.[48] While, P can also promote As release by competing for binding sites on Fe-hydroxide surfaces, with Fe plaque formation around roots found to increase P uptake.[54] It is

372 therefore, surprising that the As and Fe root tip maximum, corresponded to a significant
373 minima in P release (Figure 3), which was accompanied by a series of
374 significant/negative correlations of As or Fe with P fluxes (Table S4) across the root tip
375 zones.

376 ***Solid–Water Partitioning Contributes to Metals Mobility***. The results from DGT
377 sampling provide a direct measurement of the mean *in situ* flux from the solid phase to
378 porewater.[55] The subsoils collected specifically from soil regions with different O_2
379 concentrations showed no significant difference in their solid phase concentrations for
380 As, Pb, and Fe. However, porewater showed significant variation in As, Fe, and Mn
381 between **O-B** areas and the **O+R** zones (p<0.05) (Figure 5). Supporting the DGT
382 observations, the **O+R** zone had lower porewater concentrations. Although there was
383 some enrichment of Mn in the **O+R**, the soil-water partitioning (Kd) value was higher
384 than **O-B** regions, which is similar to the trends for As and Fe, i.e. lower element
385 solubility. Redox gradients explain the metal partitioning between these two distinct
386 areas. Some care is needed when interpreting these Kd values though, as calculation of
387 partition coefficients assume equilibrium between porewater and solid phase
388 concentration. In the presence of a growing root a true equilibrium state might not be
389 achieved fully. However, the volume of samples collected was sufficient to ensure that
390 porewaters were not just targeting zones directly at the soil-root interface.

391 At this stage in plant development there were minimal impacts on general soil
392 enrichment patterns, but significant alterations in element mobility behaviors. The oxic
393 conditions promote metal precipitation, and with the formation of Fe and Mn

394 oxyhydroxides in **O+R** zones, the increased availability of binding sites, causes a
395 corresponding decrease in the concentration of dissolved TE's in the affected soils.
396 Furthermore As, Fe, and Mn are more mobile in their reduced state, migrating strongly
397 in response to naturally occurring gradients in solute concentration towards oxidized
398 soil.[56] It is these processes from which significant changes in total element profiles
399 within the underground topsoil evolve. However, our findings of a flux maxima and a
400 decoupling of metal and P behaviors across the tip regions of rice roots indicates a
401 different chemical process, distinct to the situation occurring within the general oxygen
402 influenced rhizosphere, is dominant. This Fe flux maxima and its superimposition on
403 the outer boundary of the aerobic zone is suggestive of an overriding abiotic process. It
404 also agrees with the hypothesis that the flux arises from oxidation-mediated pH changes
405 on Fe(II) mobility.[9]

406 ***Environmental Implications.*** Understanding that the rhizosphere environment
407 greatly alters element mobilization in discrete/small localized patches is a step forward
408 in developing strategies for minimizing plant uptake and grain contamination. The
409 solute chemistries of the emergent rice rhizosphere vary from that of the surrounding
410 bulk/field soils, and we show that within these zones considerable chemical
411 heterogeneity also exists. Indeed, much of our understanding of the elemental cycling
412 within paddy fields, at least from the perspective of nutrient management/fertilizer
413 applications/soil conditioners follows the concept of homogenous, reciprocal
414 interaction, employing a chemistry where the reaction kinetics of ions/molecules are in
415 a well-mixed environment. The spatial structure of the rice rhizosphere used to be

ignored in the overall system dynamics. Indeed, the ploughed paddy topsoil does begin the cropping cycle relatively homogenized, but after flooding and overtime (0-4 months) the spatial diversity of the system increases greatly.[33] These initial first steps in solute interchange and soil surface interactions created by the emergent rhizospheres of the newly planted rice, are important because they create zones of localized enrichment/depletion in elemental bioavailability, forming different ecological niches (Figure 1), thus impacting plant uptake through diffusion and resupply. However, these gradients in porewater elements availability, later develop/establish into chemically stratified zones differing with more permanency in their solid phase composition and stoichiometry, such as is the case with Fe or Mn plaque aggregation.

In this work we capture for the first time, solute maps for As, Fe, Pb, Mn, O_2 and P, in a series of newly formed rhizospheres. We were able to validate previous observations[9] of an As and Fe flux maxima located around root apice zones at the interface between oxic-anoxic conditions, at larger spatial scales, using a variety of DGT-optode multilayer configurations, a different rice cultivar, and using a paddy soil naturally enriched in As. Moreover, we demonstrate that the flux phenomenon is common and forms predominantly around the tip regions of the upper root zone. P chemistries in the **FM** flux zone were also captured along with As, revealing a surprising disconnect between As or Fe mobilization and P release. Element distributions in porewater and subsoils demonstrate the diffusion gradient is one of the explanations for their mobilization. Further, this whole-rhizosphere demonstration of solute behaviors provides a new perspective on the development of spatial structure

438 within rice rhizospheres, a framework that can be used to further understand localized
439 patterns of element uptake and environment sensing by plant roots, microbial
440 diversity/function and critically important to As especially, speciation transformations
441 and cycling.
442

443 **ASSOCIATED CONTENT**

444 Experimental: Optode Sensor Fabrication and O_2 imaging in Rice Rhizosphere.
445 Root development assessment. QA/QC. Solid-Water Distribution Coefficient (Kd).
446 Sulfur and metals concentration in the soil by ED-XRF (Table S1); Masses of
447 analytes for ICP-MS (PerkinElmer NexION 300X) analysis to characterize laboratory
448 DGT performance (Table S2); Certified and measured concentrations of elements in
449 GBW07405 soil reference material for trace metals analysis using ED-XRF (Table S3);
450 Pearson correlation coefficient matrix of various element fluxes around the root tip on
451 PZ gel (Table S4); The results of PCA analysis corresponding with figure 1, 2/S3, and
452 3/S4 (Table S5); The distribution coefficients (Kd) of elements in different regions
453 (Table S6); The photography of root in rhizotrons (Figrue S1); Visualization of O_2, As,
454 and other elements around roots corresponding with figure 1 (Figure S2); Chemical
455 images of O_2 and elements distribution around single rice root with SPR-IDA DGT
456 corresponding with figure 2 (Figure S3); Pearson scatterplots for different elements
457 around root tips corresponding with SPR-IDA gel in figure 1 (Figure S4). Two-
458 dimensional visualization of As and other elements by ZrO DGT corresponding with
459 figure 3 (Figure S5); The physic-chemical characteristics in rice rhizosphere during

the growth stage (Figure S6).

AUTHOR INFORMATION

Corresponding Authors

*Phone: +44-0-28-9097-6539; e-mail: p.williams@qub.ac.uk (P.N.W.).

*Phone: 0086−25−89680632; e-mail: esluojun@nju.edu.cn (J.L.).

ORCID

Paul N. Williams: 0000-0002-0723-7997

Lena Q. Ma: 0000-0002-8463-9957

Jun Luo: 0000-0002-3480-8900

Notes

The authors declare no competing financial interest.

ACKNOWLEDGMENTS

This work was funded by the National Natural Science Foundation of China (No. 41771271), the Fundamental Research Funds for the Central Universities (021114380126), National Natural Science Foundation of China (No. 41807023), and Jiangsu Province Natural Science Foundation (BK20180344). The study also received support from the Newton Fund/Royal Society and NFSC (R1504GFS and 21511130063).

REFERENCES

(1) Carey, M.; Meharg, C.; Williams, P.; Marwa, E.; Jiujin, X.; Farias, J. G.; De Silva, P. M. C.; Signes-Pastor, A.; Lu, Y.; Nicoloso, F. T., Global Sourcing of Low-Inorganic Arsenic Rice Grain. *Expos. Health*

2019, 1-9.

(2) Meharg, A. A.; Williams, P. N.; Adomako, E.; Lawgali, Y. Y.; Deacon, C.; Villada, A.; Cambell, R. C.; Sun, G.; Zhu, Y.-G.; Feldmann, J., Geographical variation in total and inorganic arsenic content of polished (white) rice. *Environ. Sci. Technol.* **2009,** *43*, (5), 1612-1617.

(3) Williams, P.; Price, A.; Raab, A.; Hossain, S.; Feldmann, J.; Meharg, A. A., Variation in arsenic speciation and concentration in paddy rice related to dietary exposure. *Environ. Sci. Technol.* **2005,** *39*, (15), 5531-5540.

(4) Savage, L.; Carey, M.; Hossain, M.; Islam, M. R.; de Silva, P.; Williams, P. N.; Meharg, A. A., Elevated Trimethylarsine Oxide and Inorganic Arsenic in Northern Hemisphere Summer Monsoonal Wet Deposition. *Environ. Sci. Technol.* **2017,** *51*, (21), 12210-12218.

(5) Muehe, E. M.; Wang, T.; Kerl, C. F.; Planer-Friedrich, B.; Fendorf, S., Rice production threatened by coupled stresses of climate and soil arsenic. *Nat. Commun.* **2019,** *10*, (1), 4985.

(6) Meharg, A. A.; Hartley-Whitaker, J., Arsenic uptake and metabolism in arsenic resistant and nonresistant plant species. *New Phytol.* **2002,** *154*, (1), 29-43.

(7) Wang, P.; Zhang, W.; Mao, C.; Xu, G.; Zhao, F.-J., The role of OsPT8 in arsenate uptake and varietal difference in arsenate tolerance in rice. *J. Exp. Bot.* **2016,** *67*, (21), 6051-6059.

(8) Ma, J. F.; Yamaji, N.; Mitani, N.; Xu, X.-Y.; Su, Y.-H.; McGrath, S. P.; Zhao, F.-J., Transporters of arsenite in rice and their role in arsenic accumulation in rice grain. *Proc. Natl. Acad. Sci.* **2008,** *105*, (29), 9931-9935.

(9) Williams, P. N.; Santner, J.; Larsen, M.; Lehto, N. J.; Oburger, E.; Wenzel, W.; Glud, R. N.; Davison, W.; Zhang, H., Localized flux maxima of arsenic, lead, and iron around root apices in flooded lowland rice. *Environ. Sci. Technol.* **2014,** *48*, (15), 8498-8506.

(10) Duker, A. A.; Carranza, E.; Hale, M., Arsenic geochemistry and health. *Environ. Int.* **2005,** *31*, (5), 631-641.

(11) Seyfferth, A. L.; Webb, S. M.; Andrews, J. C.; Fendorf, S., Arsenic localization, speciation, and co-occurrence with iron on rice (Oryza sativa L.) roots having variable Fe coatings. *Environ. Sci. Technol.* **2010,** *44*, (21), 8108-8113.

(12) Yamaguchi, N.; Ohkura, T.; Hikono, A.; Yamaguchi, H.; Hashimoto, Y.; Makino, T., Effects of Iron Amendments on the Speciation of Arsenic in the Rice Rhizosphere after Drainage. *Soils* **2017,** *1*, (1), 6.

(13) Li, B.; Zhou, S.; Wei, D.; Long, J.; Peng, L.; Tie, B.; Williams, P. N.; Lei, M., Mitigating arsenic accumulation in rice (Oryza sativa L.) from typical arsenic contaminated paddy soil of southern China

using nanostructured α-MnO_2: Pot experiment and field application. *Sci. Total Environ.* **2019,** *650*, 546-556.

(14) Xu, X.; Chen, C.; Wang, P.; Kretzschmar, R.; Zhao, F.-J., Control of arsenic mobilization in paddy soils by manganese and iron oxides. *Environ. Pollut.* **2017,** *231*, 37-47.

(15) Violante, A.; Caporale, A. G., Biogeochemical processes at soil-root interface. *Journal of Soil Science & Plant Nutrition* **2015,** *15*, (2), 7.

(16) Jacob, D. L.; Otte, M. L., Long-term effects of submergence and wetland vegetation on metals in a 90-year old abandoned Pb–Zn mine tailings pond. *Environ. Pollut.* **2004,** *130*, (3), 337-345.

(17) Lee, Y. J.; Mynampati, K.; Drautz, D.; Arumugam, K.; Williams, R.; Schuster, S.; Kjelleberg, S.; Swarup, S. In *Understanding Aquatic Rhizosphere Processes Through Metabolomics and Metagenomics Approach*, EGU General Assembly Conference Abstracts, 2013; 2013.

(18) Mei, X. Q.; Wong, M. H.; Yang, Y.; Dong, H. Y.; Qiu, R. L.; Ye, Z. H., The effects of radial oxygen loss on arsenic tolerance and uptake in rice and on its rhizosphere. *Environ. Pollut.* **2012,** *165*, 109-17.

(19) Wang, M. Y.; Chen, A. K.; Wong, M. H.; Qiu, R. L.; Cheng, H.; Ye, Z. H., Cadmium accumulation in and tolerance of rice (Oryza sativa L.) varieties with different rates of radial oxygen loss. *Environ. Pollut.* **2011,** *159*, (6), 1730-6.

(20) Kuzyakov, Y.; Blagodatskaya, E., Microbial hotspots and hot moments in soil: concept & review. *Soil Biol. Biochem.* **2015,** *83*, 184-199.

(21) Chen, Z.; Zhu, Y. G.; Liu, W. J.; Meharg, A. A., Direct evidence showing the effect of root surface iron plaque on arsenite and arsenate uptake into rice (Oryza sativa) roots. *New Phytol.* **2005,** *165*, (1), 91-97.

(22) Jia, Y.; Huang, H.; Chen, Z.; Zhu, Y.-G., Arsenic uptake by rice is influenced by microbe-mediated arsenic redox changes in the rhizosphere. *Environ. Sci. Technol.* **2014,** *48*, (2), 1001-1007.

(23) Hinsinger, P.; Bengough, A. G.; Vetterlein, D.; Young, I. M., Rhizosphere: biophysics, biogeochemistry and ecological relevance. *Plant Soil* **2009,** *321*, (1-2), 117-152.

(24) Koren, K.; Brodersen, K. E.; Jakobsen, S. L.; Kühl, M., Optical sensor nanoparticles in artificial sediments–a new tool to visualize O_2 dynamics around the rhizome and roots of seagrasses. *Environ. Sci. Technol.* **2015,** *49*, (4), 2286-2292.

(25) Larsen, M.; Santner, J.; Oburger, E.; Wenzel, W. W.; Glud, R. N., O 2 dynamics in the rhizosphere of young rice plants (Oryza sativa L.) as studied by planar optodes. *Plant Soil* **2015,** *390*, (1-2), 279-292.

(26) Hinsinger, P.; Gobran, G. R.; Gregory, P. J.; Wenzel, W. W., Rhizosphere geometry and

heterogeneity arising from root-mediated physical and chemical processes. *New Phytol.* **2005,** *168*, (2), 293-303.

(27) Davison, W.; Zhang, H., In situ speciation measurements of trace components in natural waters using thin-film gels. *Nature* **1994,** *367*, (6463), 546.

(28) Zhang, H.; Zhao, F.-J.; Sun, B.; Davison, W.; Mcgrath, S. P., A new method to measure effective soil solution concentration predicts copper availability to plants. *Environ. Sci. Technol.* **2001,** *35*, (12), 2602-2607.

(29) Stahl, H.; Warnken, K. W.; Sochaczewski, L.; Glud, R. N.; Davison, W.; Zhang, H., A combined sensor for simultaneous high resolution 2-D imaging of oxygen and trace metals fluxes. *Limnology and Oceanography: Methods* **2012,** *10*, (5), 389-401.

(30) Han, C.; Ren, J.; Wang, Z.; Yang, S.; Ke, F.; Xu, D.; Xie, X., Characterization of phosphorus availability in response to radial oxygen losses in the rhizosphere of Vallisneria spiralis. *Chemosphere* **2018,** *208*, 740-748.

(31) Kreuzeder, A.; Santner, J.; Prohaska, T.; Wenzel, W. W., Gel for simultaneous chemical imaging of anionic and cationic solutes using diffusive gradients in thin films. *Anal. Chem.* **2013,** *85*, (24), 12028-12036.

(32) Davison, W.; Fones, G. R.; Grime, G. W., Dissolved metals in surface sediment and a microbial mat at 100-μm resolution. *Nature* **1997,** *387*, (6636), 885.

(33) Fang, W.; Williams, P. N.; Fang, X.; Amoah-Antwi, C.; Yin, D.; Li, G.; Ma, L. Q.; Luo, J., Field-Scale Heterogeneity and Geochemical Regulation of Arsenic, Iron, Lead, and Sulfur Bioavailability in Paddy Soil. *Environ. Sci. Technol.* **2018,** *52*, (21), 12098-12107.

(34) Das, H.; Sengupta, P.; Hossain, A.; Islam, M.; Islam, F., Diversity of environmental arsenic pollution in Bangladesh. *Bangladesh environment* **2002,** *1*, 234-244.

(35) Warnken, K. W.; Zhang, H.; Davison, W., Performance characteristics of suspended particulate reagent-iminodiacetate as a binding agent for diffusive gradients in thin films. *Anal. Chim. Acta.* **2004,** *508*, (1), 41-51.

(36) Luo, J.; Zhang, H.; Santner, J.; Davison, W., Performance characteristics of diffusive gradients in thin films equipped with a binding gel layer containing precipitated ferrihydrite for measuring arsenic (V), selenium (VI), vanadium (V), and antimony (V). *Anal. Chem.* **2010,** *82*, (21), 8903-8909.

(37) Guan, D.-X.; Williams, P. N.; Luo, J.; Zheng, J.-L.; Xu, H.-C.; Cai, C.; Ma, L. Q., Novel precipitated zirconia-based DGT technique for high-resolution imaging of oxyanions in waters and sediments. *Environ. Sci. Technol.* **2015,** *49*, (6), 3653-3661.

(38) Lehto, N. J.; Davison, W.; Zhang, H., The use of ultra-thin diffusive gradients in thin-films (DGT) devices for the analysis of trace metal dynamics in soils and sediments: a measurement and modelling approach. *Environ. Chem.* **2012,** *9*, (4), 415-423.

(39) Puy, J.; Galceran, J.; Cruz-González, S.; David, C. A.; Uribe, R.; Lin, C.; Zhang, H.; Davison, W., Measurement of metals using DGT: impact of ionic strength and kinetics of dissociation of complexes in the resin domain. *Anal. Chem.* **2014,** *86*, (15), 7740-7748.

(40) Larsen, M.; Borisov, S. M.; Grunwald, B.; Klimant, I.; Glud, R. N., A simple and inexpensive high resolution color ratiometric planar optode imaging approach: application to oxygen and pH sensing. *Limnology and Oceanography: Methods* **2011,** *9*, (9), 348-360.

(41) Kirk, G., The Biogeochemistry of Submerged Soils. **2004**.

(42) Duckworth, O. W.; Sposito, G., Siderophore-promoted dissolution of synthetic and biogenic layer-type Mn oxides. *Chemical Geology* **2007,** *242*, (3-4), 497-508.

(43) Madison, A. S.; Tebo, B. M.; Mucci, A.; Sundby, B.; Luther, G. W., Abundant porewater Mn (III) is a major component of the sedimentary redox system. *Science* **2013,** *341*, (6148), 875-878.

(44) Davison, W., Iron and manganese in lakes. *Earth-Sci. Rev* **1993,** *34*, (2), 119-163.

(45) Fones, G. R.; Davison, W.; Hamilton-Taylor, J., The fine-scale remobilization of metals in the surface sediment of the North-East Atlantic. *Cont. Shelf Res.* **2004,** *24*, (13-14), 1485-1504.

(46) Unz, R. F.; Shuttleworth, K. L., Microbial mobilization and immobilization of heavy metals. *Curr. Opin. Biotech.* **1996,** *7*, (3), 307-310.

(47) Oremland, R. S.; Stolz, J. F., The ecology of arsenic. *Science* **2003,** *300*, (5621), 939-944.

(48) Hettiarachchi, G. M.; Pierzynski, G. M.; Ransom, M. D., In situ stabilization of soil lead using phosphorus and manganese oxide. *Environ. Sci. Technol.* **2000,** *34*, (21), 4614-4619.

(49) Marschner, H.; Rimmington, G., Mineral nutrition of higher plants. *Plant, cell & environment* **1988,** *11*, (2), 147-148.

(50) Hinsinger, P., Bioavailability of soil inorganic P in the rhizosphere as affected by root-induced chemical changes: a review. *Plant Soil* **2001,** *237*, (2), 173-195.

(51) Xing, X.; Ding, S.; Liu, L.; Chen, M.; Yan, W.; Zhao, L.; Zhang, C., Direct evidence for the enhanced acquisition of phosphorus in the rhizosphere of aquatic plants: a case study on Vallisneria natans. *Sci. Total Environ.* **2018,** *616*, 386-396.

(52) Johri, A. K.; Oelmüller, R.; Dua, M.; Yadav, V.; Kumar, M.; Tuteja, N.; Varma, A.; Bonfante, P.;

Persson, B. L.; Stroud, R. M., Fungal association and utilization of phosphate by plants: success, limitations, and future prospects. *Frontiers in microbiology* **2015,** *6*, 984.

(53) Six, L.; Smolders, E.; Merckx, R., The performance of DGT versus conventional soil phosphorus tests in tropical soils—maize and rice responses to P application. *Plant Soil* **2013,** *366*, (1-2), 49-66.

(54) Xu, D.; Xu, J.; He, Y.; Huang, P., Effect of iron plaque formation on phosphorus accumulation and availability in the rhizosphere of wetland plants. *Water, air, and soil pollution* **2009,** *200*, (1-4), 79-87.

(55) Lehto, N. J.; Davison, W.; Zhang, H.; Tych, W., Analysis of micro-nutrient behaviour in the rhizosphere using a DGT parameterised dynamic plant uptake model. *Plant Soil* **2006,** *282*, (1-2), 227-238.

(56) Begg, C.; Kirk, G.; Mackenzie, A.; Neue, H. U., Root-induced iron oxidation and pH changes in the lowland rice rhizosphere. *New Phytol.* **1994,** *128*, (3), 469-477.

682

683 **Table 1. Chemical and Spatial Characteristics.** Area (cm^2) and Flux (pg cm^{-2} s^{-1})
684 measurements for rhizosphere deployed SPR-IDA DGT (Figure 1).

	Area	As	Fe	Pb	Mn
Flux Maxima (Root apex rhizosphere zones)	0.46	0.049±0.029	16.74±8.507	0.081±0.029	5.736±0.72
Aerobic Rhizosphere	6.58	0.008±0.001	2.806±0.959	0.09±0.006	4.848±0.936
Non-rhizosphere/anaerobic soil	21.5	0.009±0.003	3.193±1.226	0.09±0.007	4.632±1.032

685 Zonal element fluxes are presented as means ± standard deviation. Regions of interest included a
686 flux maxima associated with root apex rhizosphere zones (FM), aerobic rhizosphere (O+R), and
687 non-rhizosphere/anaerobic soil (O-B). The size of the three zones are 0.46, 6.58, and 21.5 cm^2,
688 containing 54, 770, and 2520 points, respectively, i.e. the deviations are derived from 54, 770, and
689 2520 replicates.
690

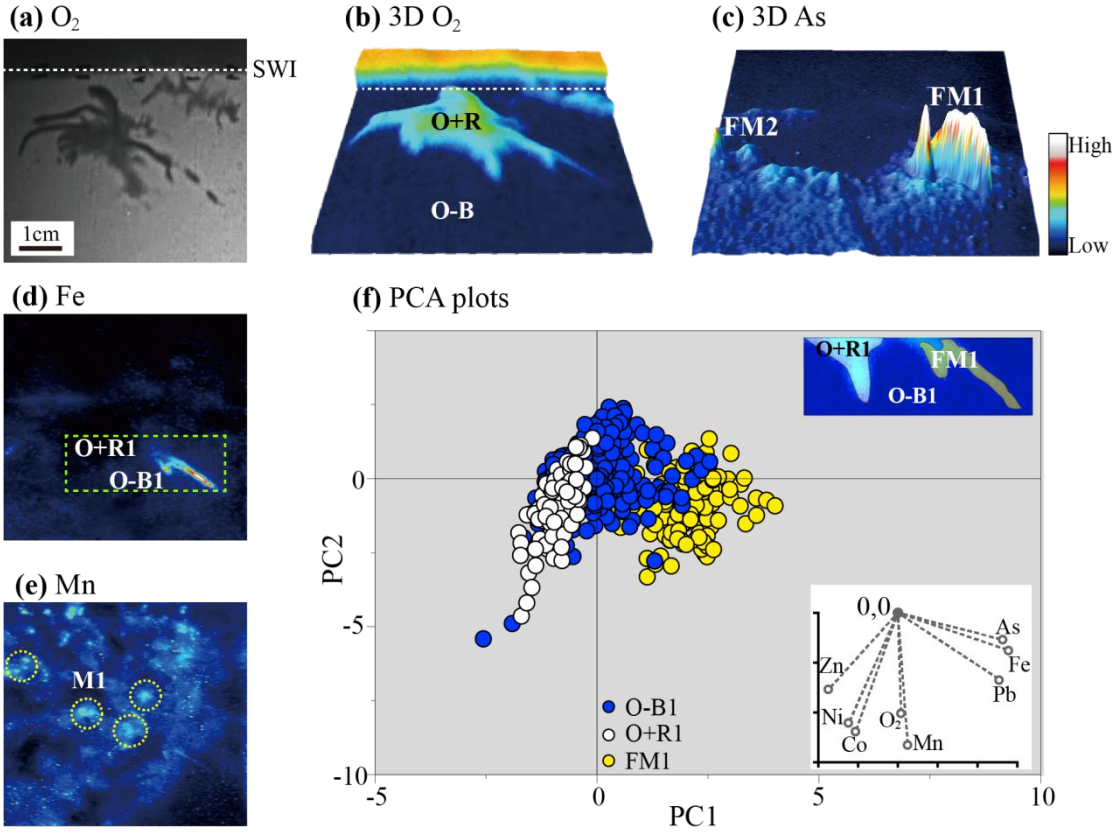

Figure 1. Solute fluxes around a set of four-week-old rice roots with SPR-IDA DGT and O_2 planar optodes. (a) image of O_2 distribution obtained before the deployment of the multilayer DGT/optode system. The horizontal dashed lines show the soil-water interface (SWI). (b) 3D plot of O_2 distribution in the rice rhizosphere, O+R denotes the aerobic rhizosphere, O-B denotes the anaerobic bulk soil. (c) 3D plot of As fluxes in rice rhizosphere. All 2D elemental plots are shown in figure S2. FM denotes the flux maxima associated with rhizosphere soil in root apex zones. (d) Fe. The green/dash-lined box shows the corresponding data extraction region/transect used for PCA analysis. (e) Mn. The yellow circles indicate flux microniches (labelled as M1) (f) PCA plot of elements in different regions, aerobic rhizosphere (O+R1), non-rhizosphere/anaerobic soil (O-B1), flux maxima in a root apex rhizosphere zone (FM1) (the original data are shown in table S5). For all images, the metal fluxes (f_{DGT}, pg cm^{-2} s^{-1}) and oxygen concentration (percent air saturation) increased sequentially with the color scale shown from blue to white. The scales in the figure represent the following ranges from 0% to 100% for O_2, from 0.004-0.126 for As, from 0-42.144 for Fe, and from 0.71 to 22.39 for Mn.

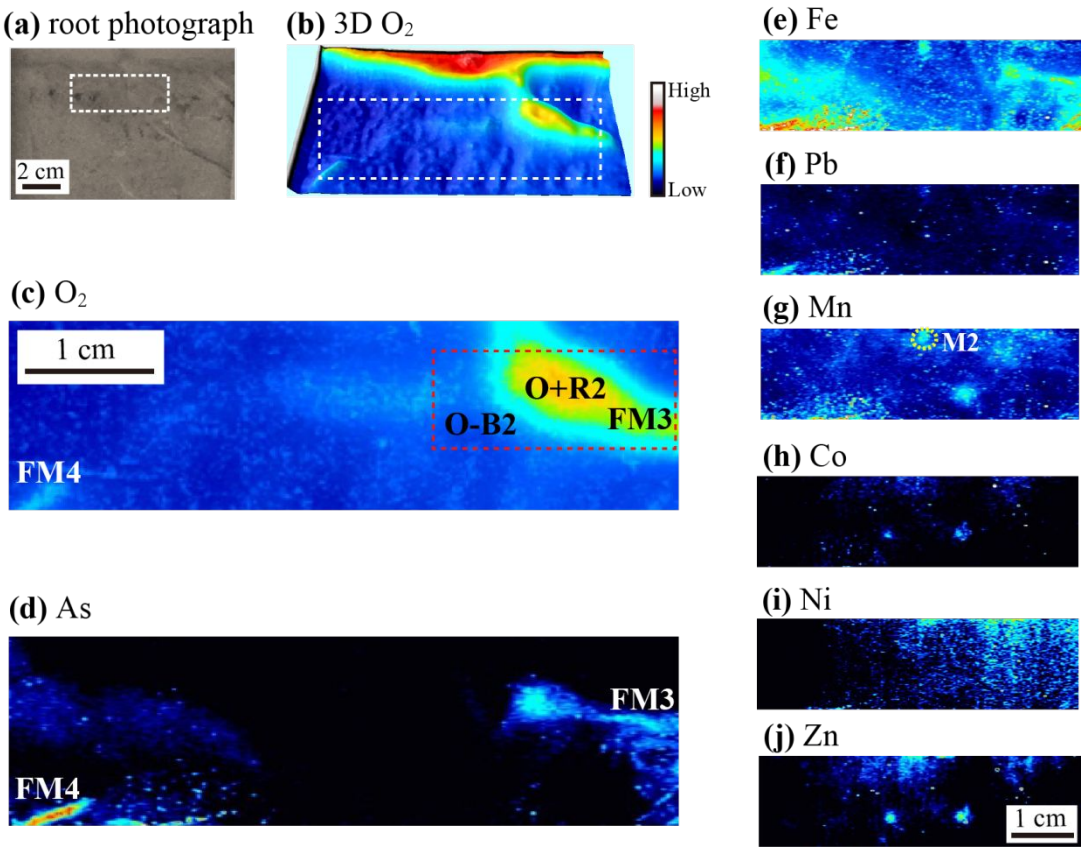

Figure 2. Root and microniche induced solute fluxes, confirmatory experiment using SPR-IDA DGT and O_2 planar optodes. Measurements were made by deploying an SPR IDA-DGT/O_2 multilayer system within a rice rhizosphere. (a) Photographic image of the soil area and the root zone subjected to chemical imaging. The white dash box shows the imaging region for O_2. (b) 3D plot of O_2 distribution in the rhizosphere. The white dash box shows the imaging region for elements. (c) 2D plot of O_2 concentration in the rhizosphere corresponding with DGT element imaging. The red/dash-lined box shows the corresponding regions for the companion PCA plot (figure S3). O+R2 denotes the aerobic rhizosphere, O-B2 denotes non-rhizosphere/anaerobic bulk soil, FM3 denotes the flux maxima associated with the root apice rhizosphere. (d) As, FM3 indicates flux maxima around root apices. (e) Fe. (f) Pb. (g) Mn, the yellow dashed circle indicates a flux microniche (label as M2). (h) Co. (i) Ni. (j) Zn. The metal fluxes (f_{DGT}, pg cm^{-2} s^{-1}) and oxygen concentration (percent air saturation) increased sequentially with the color scale shown from blue to white. The scales in the figure represent the following ranges from 0% to 100% for O_2, from 0.518-16.378 for Fe, from 0.016 to 0.046 for As, from 0-0.09 for Pb, from 0.112-0.723 for Mn, from 0.026-0.449 for Co, from 0.028-0.146 for Zn, from 0.051-0.115 for Ni.

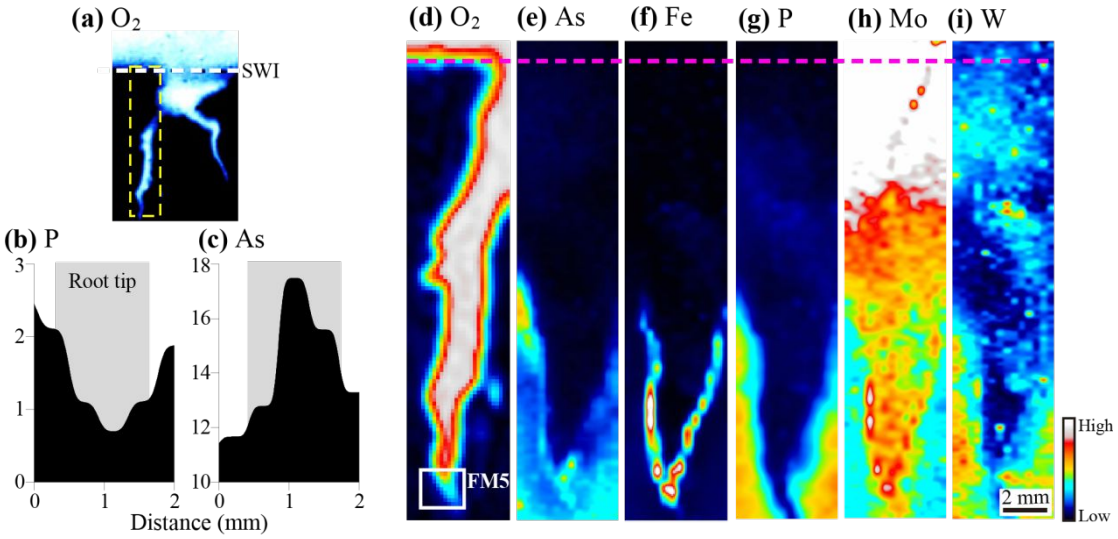

Figure 3. Chemical images of O_2 and element distribution with ZrO DGT. Element fluxes are obtained by deploying ultrathin precipitated ZrO gel in the rhizosphere for 12 h. (a) 2D O_2 distribution in the whole rhizosphere. The horizontal dashed lines show the soil-water interface (SWI). The yellow box denotes the imaging region of elements. (b) P flux transect (black shading). The grey shading indicates the root apex associated rhizosphere. (c) As flux transect (black shading). The grey shading indicates the root apex associated rhizosphere. (d) O_2 concentration around the root. The white box denotes the data extraction regions featured in the P/As biplots. (e) As (f) Fe (g) P (h) Mo (i) W. The metal/element fluxes (f_{DGT}, pg cm^{-2} s^{-1}) and oxygen concentration (percent air saturation) increased sequentially with the color scale shown from blue to white. The scales in the figure represent the following ranges from 0% to 100% for O_2, from 0.09 to 17.9 for As, from 0.42-10.27 for Fe, from 0.02-2.55 for P, from 0.17-5.62 for Mo, and from 1.24-5.87 for W. Although Mo and W images are not discussed in the text, they were included to verify/support the distinction in chemical behavior between the root apex rhizosphere zone and the bulk soil environment.

749

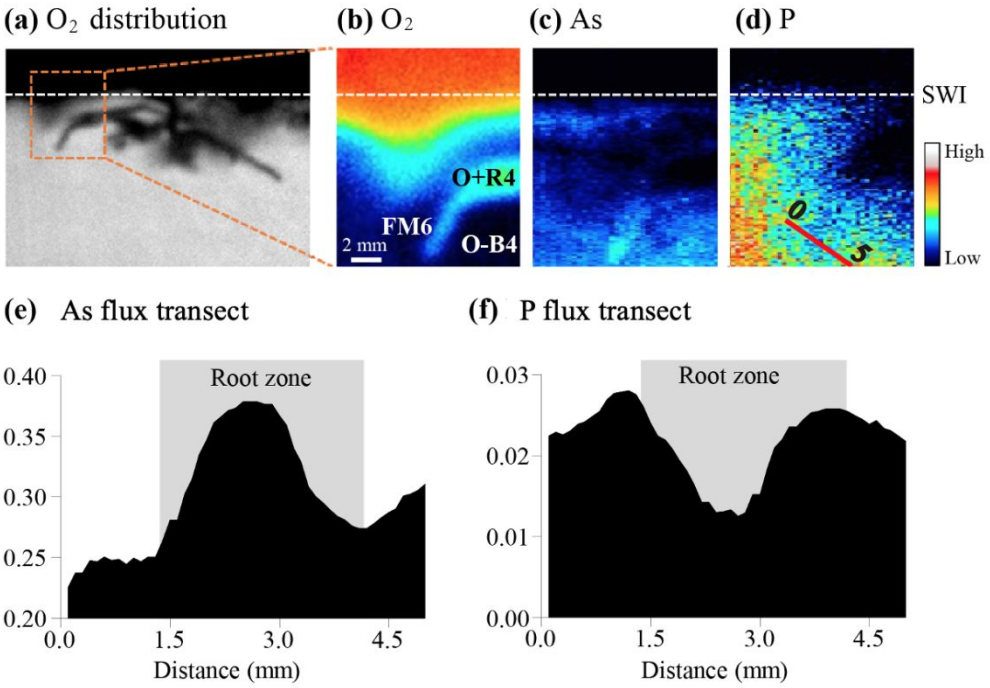

750
751

752 **Figure 4. Two-dimensional visualization of O_2, As and P in the rice rhizosphere by**
753 **PF gel.** (a) O_2 distribution in the whole plant rhizosphere. The horizontal dashed lines
754 show the soil-water interface (SWI). The orange/dash-lined box denotes the location of
755 the DGT deployment. (b) O_2 image corresponding with element imaging. O+R
756 indicates aerobic rhizosphere, O-B indicates non-rhizosphere/anaerobic bulk soil, FM
757 denotes the flux maxima from the root apex associated rhizosphere. (c) As (d) P. The
758 0, 5/bar marker shows the distance of the horizontal axes on plot (e) and (f). (e) Root
759 As flux transect (red line; subplot d). The grey shading denotes the location of the root
760 apex associated rhizosphere. (f) Root P flux transect (along the red line). The grey
761 shading denotes the location of the root apex associated rhizosphere. The metal fluxes
762 (f_{DGT}, pg cm^{-2} s^{-1}) and oxygen concentration (percent air saturation) on the 2D images
763 increased sequentially with the color scale shown from blue to white. The scales in the
764 figure represent the following ranges from 0% to 100% for O_2, from 0.016 to 0.378 for
765 As, and from 0.003-0.041 for P.
766

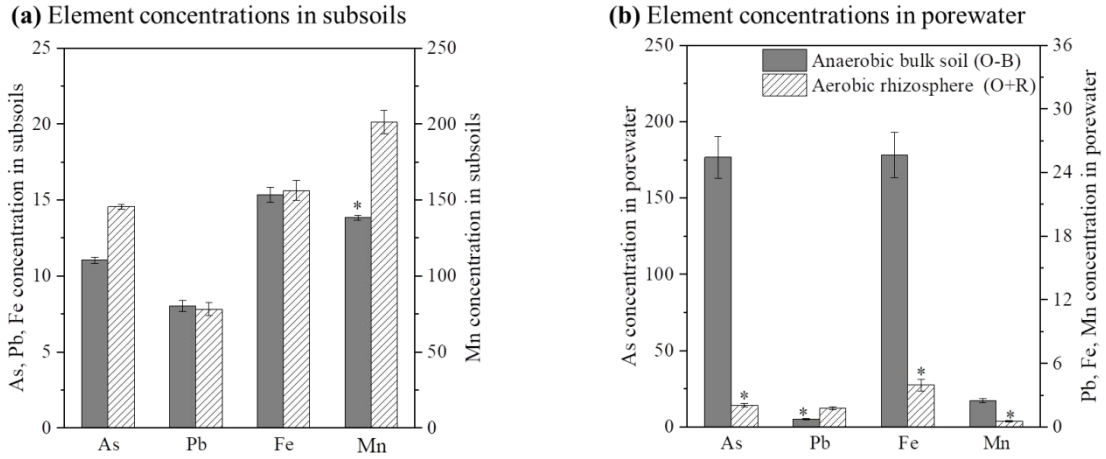

Figure 5. Concentrations of As, Pb, Fe and Mn in subsoils (a) and porewater (b) from anaerobic bulk/field zone (O-B) and rhizosphere aerobic zone (O+R). The error bars are from the standard error of 6 replicates. Note the concentration units- unit of Fe in subsoils is g kg^{-1}, As, Pb, and Mn in subsoils is mg kg^{-1}. The unit of Fe and Mn in porewater is mg l^{-1}, As and Pb in porewater is µg l^{-1}. The asterisks (*) denote significant difference at $p< 0.05$ evaluated by one-way analysis of variance followed by Duncan's multiple range test between bulk anaerobic media and rhizosphere aerobic zone.